Tunability of the dielectric response of epitaxially strained $SrTiO_3$ from first principles

Armin Antons,* J. B. Neaton,† Karin M. Rabe, and David Vanderbilt
Department of Physics and Astronomy, Rutgers University, Piscataway, New Jersey 08854-8019, USA
(Received 23 June 2004; revised manuscript received 1 November 2004; published 13 January 2005)

The effect of in-plane strain on the nonlinear dielectric properties of $SrTiO_3$ epitaxial thin films is calculated using density-functional theory within the local-density approximation. Motivated by recent experiments, the structure, zone-center phonons, and dielectric properties with and without an external electric field are evaluated for several misfit strains within ±3% of the calculated cubic lattice parameter. In these calculations, the in-plane lattice parameters are fixed, and all remaining structural parameters are permitted to relax. The presence of an external bias is treated approximately by applying a force to each ion proportional to the electric field. After obtaining zero-field ground state structures for various strains, the zone-center phonon frequencies and Born effective charges are computed, yielding the zero-field dielectric response. The dielectric response at finite electric field bias is obtained by computing the field dependence of the structure and polarization using an approximate technique. The results are compared with recent experiments and a previous phenomenological theory. The tunability is found to be strongly dependent on the in-plane lattice parameter, showing markedly different behavior for tensile and compressive strains. Our results are expected to be of use for isolating the role of strain in the tunability of real ultrathin epitaxial films.

DOI: 10.1103/PhysRevB.71.024102 PACS number(s): 77.55.+f, 77.84.Dy, 77.22.Ej

I. INTRODUCTION

Microwave dielectric materials strongly tunable by the application of an electric bias field are increasingly important for a variety of applications in microwave electronics, including tunable capacitors and oscillators, phase shifters, and delay lines.[1–3] The dependence of dielectric constant ϵ on bias field $\mathcal{E}$ is typically strongly nonlinear, and a tunability parameter n can be defined as $n=[\epsilon(0)-\epsilon(\mathcal{E})]/\epsilon(0)$, where $\mathcal{E}$ is an operational bias field of interest. Because of the potential technological impact, considerable experimental effort has been directed toward the design, control, and optimization of highly tunable low-loss materials.

For many applications, thin-film morphologies are required, and in recent years the growth of high-quality ultrathin perovskite films with unprecedented atomic-level control has become possible, using techniques such as molecular-beam epitaxy (MBE)[4] and pulsed-laser deposition (PLD).[5] These efforts have achieved the growth of single-crystal films of nanometer-scale thickness with a minimum of defects. Even so, the dielectric properties of these films often differ quite substantially from bulk.[6,7] This difference is due to a number of factors, of which the strain in the film is in many cases among the most important. More specifically, the mechanical boundary conditions on a coherent epitaxial film require the in-plane lattice constant of the film to stretch (or contract) to match the lattice constant of the substrate. Both experimental and theoretical studies have found that even small epitaxial strains can appreciably influence the Curie temperature and the dielectric permittivity and tunability of $BaTiO_3$, $SrTiO_3$, and $Ba_{1-x}Sr_xTiO_3$ (BST) thin films.[8–11]

Paraelectric BST at x near 0.5 is already known to possess a large dielectric response and high tunability at room temperature, associated with close proximity to the ferroelectric phase transition at about −23 K (Ref. 12). However, significantly lower loss has been reported for single-crystal $SrTiO_3$ (STO) thin films,[13] possibly due to the absence of compositional disorder. The ground state of STO is nonpolar but nearly ferroelectric, and thus small applied stresses would be expected to have a significant influence on the Curie temperature and associated susceptibilities. Indeed, recent experimental studies[14,15] indicate that significant changes in Curie temperature and dielectric properties occur when STO is grown epitaxially on substrates with different lattice constants. Haeni *et al.*[15] report a shift of the ferroelectric (FE) transition temperature to $T_c \approx 293$ K for a $SrTiO_3$ film of thickness 500 Å grown on (110)-oriented $DyScO_3$, corresponding to a biaxial tensile strain of 0.8%. Hyun and Char have fabricated epitaxial $SrTiO_3$ heterostructures with in-plane lattice constants below as well as above the bulk $SrTiO_3$ lattice constant, and have measured dielectric properties depending on lattice mismatch.[14] They report a general trend of increasing out-of-plane dielectric constants and higher tunability with increasing tetragonality, i.e., with decreasing in-plane lattice constant.

One of the best-studied perovskite materials, pure STO is the subject of considerable experimental and theoretical literature. STO adopts the centrosymmetric cubic perovskite structure at room temperature, and undergoes a structural phase transition from the cubic to a tetragonal, nonpolar antiferrodistortive (AFD) phase when cooled below 105 K.[16] This transition, however, is observed to have little effect on the dielectric properties. Cooling to still lower temperatures results in a strong Curie-Weiss-type increase in the static dielectric response, suggestive of a phase transition at about 20 K. However, no transition actually occurs in that temperature range; instead, the dielectric constant saturates to a value of $\sim 2\times 10^4$ at zero temperature.[17–23] The absence of the FE transition can be explained by quantum fluctuations of the atoms about their centrosymmetric cubic positions (i.e., the formation of a "quantum paraelectric" state).[19–22,24,25] The proximity to a ferroelectric transition is also evident from experiments showing that modest uniaxial stress is capable of inducing ferroelectricity.[26] Several first-principles[22,23,27–29]

and classical Monte Carlo simulations on an effective Hamiltonian[30] have already provided valuable insight into the structural properties and temperature dependence of FE phase transitions in bulk STO. In particular, the interaction between FE and AFD instabilities in the bulk phase has been thoroughly studied from first principles by Sai and Vanderbilt.[31] Moreover, a previous phenomenological study of the effects of epitaxial strain on STO thin films by Pertsev *et al.*,[32] based on a Landau theory fit to experimental data from bulk phases, produced a rich temperature-strain phase diagram and provided support for the idea that the oxygen-octahedron rotations have little influence on the dielectric response.

In this work, we compute the effects of the in-plane epitaxial lattice-matching constraint on the dielectric response and tunability of $SrTiO_3$ using first-principles density-functional theory within the local-density approximation (LDA). Since there is only a small change in the dielectric response of bulk $SrTiO_3$ as the temperature is lowered through the AFD transition temperature of 105 K, we believe it is a reasonable first approximation to adopt a theory that neglects the AFD instabilities, as we have done here. We also restrict our analysis to zero temperature, but for simplicity we neglect the quantum fluctuations. Thus, our focus will be on the ferroelectric soft mode and its coupling to strain. Despite these restrictions, the fact that we use a first-principles approach means that we do not have to rely on empirical Landau parameters as in Ref. 32. Thus, we can confidently make predictions under conditions that vary drastically from those under which the data determining the parameters were obtained, allowing us to consider the effects of large epitaxial strains and finite electric fields.

There is one major limitation of our theory, connected with the fact that the LDA tends to underestimate lattice constants. Because compression tends to suppress ferroelectricity, this means that our LDA system is "less ferroelectric" than true STO at zero temperature. Indeed, we report below a soft-mode frequency of about 75 cm^{-1} and a dielectric constant of about 390 at zero temperature for unstrained STO within the LDA, whereas the experimental zero-temperature system is exquisitely close to the ferroelectric transition with $\omega_{soft} \simeq 10$ cm^{-1} and $\epsilon \simeq 20\,000$.[26] However, raising the temperature also has the effect of suppressing the ferroelectric instability, so that the experimental system *at room temperature* is characterized by $\omega_{soft} \simeq 90$ cm^{-1} and $\epsilon \simeq 290$. Thus, fortuitously, the zero-temperature LDA system corresponds reasonably well with the real physical system at a temperature near, or a bit below, room temperature. Comparisons between these systems must obviously be approached with caution, but in fact we find good semiquantitative agreement for several of the physical properties of these two corresponding systems as will be presented below.

The manuscript is organized as follows: In Sec. II, we provide the details of our approach and approximations used, including our handling of finite electric fields. In Sec. III, we present and discuss the results of our calculations for epitaxially strained STO, with emphasis on the strain dependence of the tunability by finite electric fields. Our conclusions appear in Sec. IV.

II. METHOD

A. First-principles calculations

First-principles density-functional calculations are performed within the local-density approximation (LDA) as implemented in the PWSCF package.[34] The exchange-correlation energy is evaluated using the Ceperley-Alder form with Perdew-Zunger parameterization. Vanderbilt ultrasoft pseudopotentials[35] are used treating 10 electrons as valence for Sr ($4s^2 4p^6 5s^2$), 12 electrons for Ti ($3s^2 3p^6 4s^2 3d^2$), and 6 for O ($2s^2 2p^4$). To achieve well-converged results for small changes in the lattice constant, the electronic wave functions are expanded in plane waves up to a kinetic energy of 50 Ry. All calculations are performed with a $6\times6\times6$ Monkhorst-Pack **k**-point mesh.[36] To establish minimum-energy configurations we converged the Hellmann-Feynman forces acting on the atoms to less than 0.1 mRy/a.u. Density functional perturbation theory (DFPT) is then used to calculate the phonon frequencies of the structural optimized systems.

B. Structural constraints

The role of epitaxial strain on the structural properties of STO is isolated by systematically seeking the ground-state structure of five-atom unit cells of *bulk* STO constrained to several different in-plane lattice constants, differing from the theoretical cubic lattice constant by fractions ranging between −3% and +3% in steps of 0.5%, and allowing all atomic positions and the perpendicular lattice constant to relax fully until the energy is minimized. To locate the phase transition points, and for the electric field calculations, the in-plane lattice constant was varied in smaller steps of 0.1% in the paraelectric region. The presence of the strain necessarily lowers the symmetry of the cubic STO system to tetragonal at most; further spontaneous symmetry reduction occurs for certain ranges of lattice constant. In the remainder of this subsection, we provide specific details of each of the structures considered in this work and introduce the relevant notation.

1. Epitaxial strains near zero

The zero-strain paraelectric phase of $SrTiO_3$ has the ideal cubic $Pm\bar{3}m$ perovskite structure, in which the octahedral oxygen atoms lie at Wyckoff 3c positions $\left(\frac{1}{2},\frac{1}{2},0\right)$, a single Ti atom lies at the body-centered site 1b $\left(\frac{1}{2},\frac{1}{2},\frac{1}{2}\right)$, and the lone Sr cation is at 1a $(0,0,0)$. Our calculations result in a theoretical lattice constant a of 7.285 a.u., i.e., ~1.1% less than the experimental value of 7.365 a.u.; this underestimate is expected when using the LDA and is consistent with several previous LDA-based studies.

For small tensile or compressive strains, the structure of STO remains centrosymmetric, but the symmetry is lowered to tetragonal (space group $P4/mmm$). In this "pseudocubic" phase, the cations sit at Wyckoff positions 1a $(0,0,0)$ for Sr and 1d $\left(\frac{1}{2},\frac{1}{2},\frac{1}{2}\right)$ for Ti. There are two different Wyckoff positions for oxygen: 1c $\left(\frac{1}{2},\frac{1}{2},0\right)$, which will be referred to as $O_\perp$ (in the Ti-O chain along [001]), and 2e $\left(0,\frac{1}{2},\frac{1}{2}\right),\left(\frac{1}{2},0,\frac{1}{2}\right)$

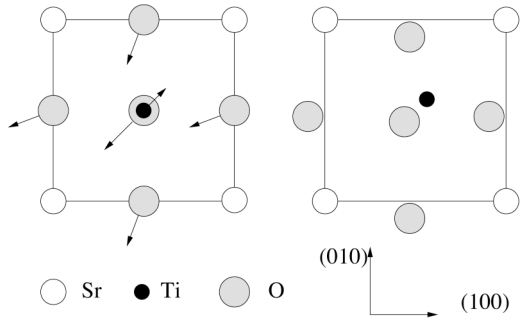

FIG. 1. Left: Sketch of atomic displacements (arrows) giving rise to the ferroelectric *Amm*2 structure under tensile strain, shown in [001] projection. (Sr atoms are fixed by definition.) Lengths and angular deviations of the arrows are exaggerated for clarity, but the relative sizes and directions of the displacements are qualitatively correct. Right: Schematic view of resulting structure.

which will be referred to as $O_{\|x}$ and $O_{\|y}$ and lie in the same (001) plane as Ti.

2. Compressive epitaxial strains

For large enough compressive epitaxial strains, the symmetry of the tetragonal phase is found to be lowered further to noncentrosymmetric *P*4*mm*. This is a ferroelectric tetragonal structure with polarization along [001]. The Wyckoff positions are 1a $(0,0,z=0)$ for Sr, 1b $\left(\frac{1}{2},\frac{1}{2},\frac{1}{2}+\Delta \mathrm{Ti}_z\right)$ for Ti, 1b $\left(\frac{1}{2},\frac{1}{2},\Delta \mathrm{O}_{\perp z}\right)$, and 2c $\left(\frac{1}{2},0,\frac{1}{2}+\Delta \mathrm{O}_{\|z}\right)$ for oxygens. The presence of a zone-boundary instability associated with rotation of the oxygen octahedra has been discussed for this phase in earlier work,[28,37] and will not be considered further here.

3. Tensile epitaxial strains

Above a critical value of tensile epitaxial strain, STO becomes ferroelectric and transforms to an orthorhombic *Amm*2 structure. This structure is noncentrosymmetric, exhibiting a nonzero polarization along [110]. The Wyckoff positions associated with this phase are 2a $(z=0,0,0)$ for Sr, 2b $\left(\frac{1}{2}+\Delta \mathrm{Ti}_x,0,\frac{1}{2}\right)$ for Ti, and 2b $\left(\frac{1}{2}+\Delta \mathrm{O}_{\perp x},0,0\right)$ and 4e $\left(\frac{1}{4}+\Delta \mathrm{O}_{\|x},\frac{1}{4}+\Delta \mathrm{O}_{\|y},\frac{1}{2}\right)$ for oxygens. The structure is illustrated in Fig. 1. The cell-doubling oxygen-octahedron rotation expected for this phase[32] will not be considered in the remainder of this paper.

C. Electric field

1. Field-induced forces

To describe the dielectric behavior of STO under finite dc bias, we must evaluate its properties in the presence of a homogeneous electric field. This turns out to be subtle; fully first-principles methods for computing the behavior of periodic systems in finite fields have only recently been developed and are still in their nascent stages.[38,39] For STO, we resort to a simple and effective approximate technique that consists of first computing the Born effective charge tensors Z_i^* for each of the ions i, and then adding a term $-eZ_i^*\mathcal{E}$ to their Hellmann-Feynman forces $\mathbf{f}_i$, where e is the electronic charge and is defined to be positive. The structure is relaxed until the total force on each atom is close to zero, i.e., until $\mathbf{f}_i=-eZ_i^*\mathcal{E}$. Similar approximations were discussed by Rabe[40] and then implemented and used by Sai, Rabe, and Vanderbilt;[37] this approximation was also recently used by Fu and Bellaiche.[41]

To be more precise, we ideally would determine the structure of STO by minimizing, with respect to first wave functions $\psi_{n\mathbf{k}}$ and then to atomic coordinates $\mathbf{u}_i$, the electric enthalpy $\mathcal{F}$ per unit cell,

$$\mathcal{F}(\mathcal{E}) = E_{KS} - \Omega \mathbf{P}\cdot\mathcal{E}, \tag{1}$$

where E_{KS} is the internal energy obtained from a Kohn-Sham functional (e.g., within the local-density or generalized-gradient approximation),[38,42] $\mathbf{P}=\mathbf{P}_{\mathrm{ion}}+\mathbf{P}_{\mathrm{el}}$ is the total (ionic plus electronic) macroscopic polarization, $\mathcal{E}$ is the electric field, and Ω is the volume of the unit cell. E_{KS} and $\mathbf{P}$ are explicit functions of atomic coordinates $\mathbf{u}_i$ and wave functions $\psi_{n\mathbf{k}}$, with the electric field $\mathcal{E}$ entering into $\mathcal{F}$ only through multiplication of the functional $\mathbf{P}$. (Of course, $\mathcal{F}, E_{\mathrm{KS}}$, and $\mathbf{P}$ can also be regarded as implicit functions of $\mathcal{E}$ through the dependence of the equilibrium values of the $\psi_{n\mathbf{k}}$ upon $\mathcal{E}$.) By a Hellmann-Feynman argument,[38] the total force acting on an ion is

$$-\frac{\partial E_{\mathrm{KS}}}{\partial \mathbf{u}_i}+\Omega\frac{\partial \mathbf{P}}{\partial \mathbf{u}_i}\cdot\mathcal{E}=\mathbf{f}_i+Z_i^*e\cdot\mathcal{E}, \tag{2}$$

where the Z_i^* are the Born effective charges; these also depend implicitly on $\mathcal{E}$, even at fixed $\mathbf{u}_i$, via the $\psi_{n\mathbf{k}}(\mathcal{E})$.

Here, we neglect the field dependence of $\mathbf{f}_i$ and Z_i^*, computing these at $\mathcal{E}=0$, so that the field enters only explicitly as the multiplier of Z_i^*e in Eq. (2). This is essentially the approximation introduced in Ref. 37. Although we are able to compute the nonlinear behavior of the structural and dielectric properties insofar as they arise via field-induced lattice displacements, we neglect purely electronic nonlinearities. Thus, the results are rigorously correct only to first order in the field.[37]

2. Modeling in a reduced subspace

In practice, we find that a straightforward minimization of $\mathcal{F}$ using the forces of Eq. (2) leads to numerical instabilities when the system is close to a second-order phase transition. This problem arises because the energy surface has a very shallow minimum (or competing minima and saddle points) and the Hessian matrix becomes poorly conditioned. These numerical difficulties can be solved by identifying a subspace that spans, to a good approximation, the space of field-induced structural distortions, and then parameterizing the energy in this subspace. This modeling also helps us better understand the nonlinear effects of the field on the structure and dielectric properties.

To identify the relevant subspace, we begin by finding the pattern of atomic displacements produced by an infinitesimal electric field; it is obtained by multiplying the inverse of the

force constant matrix $\phi_{ij,\alpha\beta}$ with the forces $f_{i,\alpha}=-e\Sigma_\beta Z_{i,\alpha\beta}\mathcal{E}_\beta$. Explicitly, the displacement $u_{i,\alpha}$ of atom i in Cartesian direction α is

$$u_{i,\alpha} = -\sum_{j,\beta} \phi^{-1}_{ij,\alpha\beta} f_{j,\beta}. \tag{3}$$

In this work we will consider electric fields applied exclusively along the $\hat{z}$ direction, perpendicular to the substrate assuming an (001) film, so the sum over β above is reduced to a single term. We focus our attention in this part of the work on two structures ($P4/mmm$ and $Amm2$); for these (as well as for $P4mm$, which we will not consider further) the symmetry is such that the forces and displacements are also only along $\hat{z}$. Thus, Cartesian indices are dropped for the remainder of this subsection, with all quantities referring implicitly to $\hat{z}$ components only.

Once these displacements u_i have been found, an expression for the electric enthalpy $\mathcal{F}(\mathcal{E})$ is obtained as follows. We gather the u_i into a n-dimensional vector ξ normalized to unity. (Here n is the number of atoms in the unit cell; $n=5$ for STO.) For each misfit strain, ξ defines the subspace of possible field-induced displacements. The field dependence of the structure and polarization obtained in this model are then that obtained by relaxing the ions and minimizing the electric enthalpy subject to the constraint that the atomic displacements lie along ξ. This should be a very good approximation for small displacements considered here.

After constructing ξ, we express the electric enthalpy in terms of the scalar amplitude u. Keeping terms only to fourth order, we obtain

$$\mathcal{F}(u) = E_0 + bu^2 + du^4 - \Omega\Delta P\mathcal{E} = E_0 + bu^2 + du^4 - u\sum_i \xi_i \overline{Z_i^*}\mathcal{E}. \tag{4}$$

Here $\overline{Z_i^*}$ is the mode effective charge given below in Eq. (9), computed at zero field and for the zero-field structural parameters. For each misfit strain, the amplitude u was varied up to $0.03c$ in steps of $0.002c$ (where c is the lattice constant perpendicular to the implied substrate) to obtain the expansion coefficients b and d in Eq. (4).[43]

The electric field corresponding to a given u is then extracted from the equilibrium condition

$$\frac{\partial E}{\partial u} = 2bu + 4du^3 - \sum_i \xi_i \overline{Z_i^*}\mathcal{E} = 0. \tag{5}$$

This leads to

$$\mathcal{E}(u) = \frac{2bu + 4du^3}{\Sigma_i \xi_i \overline{Z_i^*}}. \tag{6}$$

Thus, having computed the quantities $P, \mathcal{E}$, and $\mathcal{F}$ on a mesh of u values, we obtain parametric relations between these quantities that can be plotted to reveal the dielectric behavior of interest in a numerically stable way.

D. Dielectric response and tunability

The dielectric function in the frequency range of the optical phonons can be written as the sum of electronic and phonon contributions, that is,

$$\boldsymbol{\epsilon}(\omega) = \boldsymbol{\epsilon}^\infty + \boldsymbol{\epsilon}^{\mathrm{ph}}(\omega). \tag{7}$$

In most insulating perovskite oxides (ferroelectrics and related materials), the electronic contribution is rather small ($\boldsymbol{\epsilon}^\infty \sim 5$) and constant, and the static dielectric constant $\boldsymbol{\epsilon}^0 = \boldsymbol{\epsilon}(0)$ is typically in the range of 20–100, so the phonon contribution is expected to dominate. In this work, we restrict our focus to the static dielectric response and its tunability; we calculate and analyze the phonon contribution, neglecting $\boldsymbol{\epsilon}^\infty$. For the remainder of the paper, we drop the superscripts and use the generic term dielectric response, even though we only compute the phonon contribution. Thus, in what follows, the dielectric constant $\boldsymbol{\epsilon}$ has the meaning of $\boldsymbol{\epsilon}^{\mathrm{ph}}(0)$.

At zero bias, the zero-frequency phonon response is calculated in a straightforward manner using density functional perturbation theory (DFPT) to obtain the zone-center IR-active phonon modes and their frequencies, and using the Berry-phase theory of polarization[44] to compute Born effective charges by finite differences. To evaluate the static response in an applied field, and thus the tunability, we use the subspace approach presented in Sec. II C 2 above, which greatly simplifies our treatment while retaining a high degree of accuracy. In the following, both methods are described in detail.

1. Zero dc bias

In the absence of an electric field, the lattice contribution to the static dielectric permittivity tensor $\boldsymbol{\epsilon}_0$ can be written

$$\boldsymbol{\epsilon}^{\mathrm{ph}}_{\alpha\beta} = \sum_m \frac{4\pi e^2}{M_0\Omega} \frac{\tilde{Z}^*_{m\alpha}\tilde{Z}^*_{m\beta}}{\omega_m^2}, \tag{8}$$

which includes a contribution from each of the zone-center polar modes m. Here, Ω is the volume of the primitive unit cell, M_0 is a reference mass taken as 1 amu, and $\tilde{Z}^*_{m\alpha}$ is the mode effective charge,

$$\tilde{Z}^*_{m\alpha} = \sum_{i\gamma} Z^*_{\alpha\gamma}(i) \sqrt{\frac{M_0}{M_i}} \hat{e}_m(i\gamma), \tag{9}$$

where $\hat{e}_m(i\gamma)$ is a dynamical matrix eigenvector. The corresponding real-space eigendisplacement of atom i along γ is given by $\hat{u}_m(i\gamma) = \hat{e}_m(i\gamma)/\sqrt{M_i}$. The Born effective charge $Z^*_{\alpha\gamma}(i)$ is given by

$$Z^*_{\alpha\gamma}(i) = \frac{\Omega}{|e|} \frac{\partial P_\alpha}{\partial u_{i\gamma}}. \tag{10}$$

In practice, we evaluate the effective charges by finite differences, computing the change in polarization ΔP induced by several small mode amplitudes $\Delta u_{i\gamma}$ via the Berry-phase approach using a $6\times6\times20$ **k**-point mesh.

2. Nonzero dc bias

To calculate the lattice contribution to the static dielectric constant in an applied electric field, we use the subspace approach presented in Sec. II C 2. The field-induced change in the structure is specified by a single parameter u, which determines the atomic displacements through the normalized displacement vector ξ. We express the lattice contribution to the dielectric susceptibility in terms of the change in polarization induced by an applied electric field,

$$\chi(\mathcal{E}) = \frac{dP(\mathcal{E})}{d\mathcal{E}} = \frac{dP}{du}\frac{du}{d\mathcal{E}} = \left(\sum_i \xi_i \overline{Z_i^*}\right)\frac{du}{d\mathcal{E}}. \qquad (11)$$

The expression $\epsilon = 1 + 4\pi\chi(\mathcal{E})$ is used to convert susceptibility to dielectric constant. In practice, the derivative $du/d\mathcal{E}$ is calculated numerically once $\mathcal{E}(u)$ is determined from Eq. (6). For strains close to the phase boundary, the zero-field dielectric constant computed in this manner is identical, by construction, to that obtained in Sec.II D 1 using DFPT to obtain phonon frequencies and eigenvectors, and the Berry-phase calculations to obtain Born effective charges. Furthermore, for strains where the parameter b was fit to energies for finite u, as described in Sec.II C 2, the zero-field dielectric constant is in excellent agreement with the DFPT results. To obtain the tunability, we compute the dielectric response for an appropriate range of values of $\mathcal{E}(u)$.

Note that the dielectric constants calculated here are obtained at constant strain, both in-plane and out-of-plane. The fact that we do not relax the out-of-plane strain (equilibrium c/a) with changing electric field is an additional approximation of our theory. However, because the system is paraelectric, the errors introduced by this approximation should be small, vanishing at zero bias and appearing only linearly as the electric bias field is increased, with a constant of proportionality that is related to the electrostriction constant evaluated at zero field. Thus, this approximation essentially corresponds to the neglect of electrostriction effects, which we expect to be small.

III. RESULTS AND DISCUSSION

A. Response to epitaxial strain

1. Structural properties

As described in Sec.II B, we first find the minimum-energy structure of $SrTiO_3$ for values of the misfit strain between −3% and +3%. For compressive strains larger than 0.75%, the lowest-energy structure is ferroelectric tetragonal $P4mm$, with polarization along [001]. At −0.75%, there is a continuous transition to the nonpolar tetragonal $P4/mmm$ phase. At +0.54%, there is another continuous transition to the ferroelectric orthorhombic $Amm2$ structure, with polarization along [110].

Figure 2 shows the polarization along [001] and [110] directions. The polarization increases dramatically with strain, and for large strains above 2% (tensile or compressive), the magnitude of the polarization becomes comparable to that of bulk $BaTiO_3$, a prototypical ferroelectric. This suggests that by simply choosing the appropriate substrate, the polarization of thin ferroelectric STO films, when under short-circuit electrical boundary conditions, could be tuned to a wide range of values.

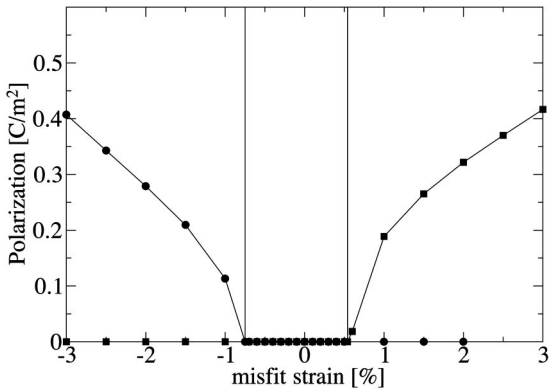

FIG. 2. Polarization as a function of misfit strain. Solid circles and squares denote polarization along [001] and [110], respectively.

In Fig. 3 we show the c/a ratio as a function of misfit strain. For tensile (positive) misfit strains, c/a drops almost linearly as the magnitude of the misfit strain increases and is largely unaffected by the development of the in-plane ferroelectric instability at the transition to the $Amm2$ phase. For compressive epitaxial strains, in contrast, a noticeable nonlinearity emerges when approaching the transition to the $P4mm$ phase; this may be indicative of the mounting structural frustration that is eventually relieved by the occurrence of the transition. Once the phase boundary has been crossed, the onset and growth of the c-axis polarization in the $P4mm$ phase further increases the c/a ratio, and c/a once again becomes very nearly linear with misfit strain in the strongly compressive regime. Also shown in Fig. 3 are some measurements of Hyun and Char[14] at 77 K that, while noisy, show a trend that is roughly consistent with the theory, as will be discussed further in Sec. III B 2.

It is of interest to compare our misfit phase diagram with that of Pertsev *et al.*[32,33] The latter is obtained by expressing the free energy as a function of misfit strain, temperature, polarization, and several additional order parameters corresponding to the linear oxygen displacements that account for

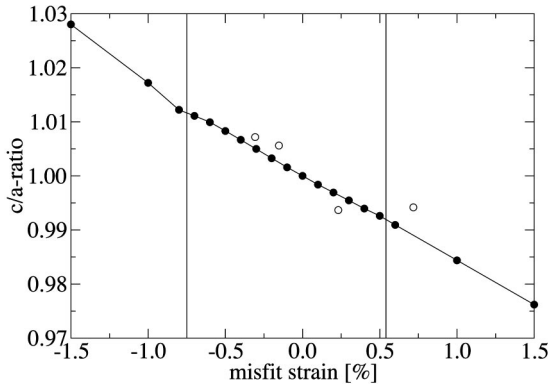

FIG. 3. Calculated c/a as a function of misfit strain in $SrTiO_3$. The behaviors for $c/a < -1.5\%$ and $c/a > +1.5\%$ (not shown) are very nearly given by linear extrapolation. The open circles denote the samples measured by Hyun and Char (Ref. 14).

possible rotations of the oxygen octahedra. The parameters in this Landau-theory expression are obtained phenomenologically. Relative to the Landau theory, our results should generally become more accurate for higher strain states, since the extrapolation from the empirical fits performed at zero strain can be expected to become less reliable there.

Regarding the nature of the polarization in the sequence of phases at zero temperature, the present first-principles results are in very good agreement with the Landau analysis. There are several detailed differences, however. First, our window of strains over which the system remains paraelectric (between −0.75% and +0.54%) is noticeably wider than that previously obtained (between −0.2 and −0.02% in Refs. 32 and 33). Our overestimate of the stability of the paraelectric phase can largely be attributed to the LDA. Specifically, since our zero-temperature calculations within the LDA result in a slightly smaller lattice constant than experiment, and since the smaller volume stabilizes the paraelectric phase, our description of the bulk system yields a more stable paraelectric phase, as our underestimate of the bulk static dielectric constant attests (calculated ~400 compared to the $\sim 2\times 10^4$ observed experimentally). In addition, octahedral rotations, not included in our analysis, might also alter the critical strain corresponding to the FE phase transitions in this region.

Another difference between the present work and Refs. 32,33 is the prediction in the latter of a low-temperature [100]-polarized ferroelectric phase under in a narrow window of tensile strain. Our results are consistent with only a single phase in this strain regime, with a polarization along [110]. Their polar [100]-oriented orthorhombic phase might be stabilized by the rotations not included here, but since it occurs only in a very small strain region, we did not investigate it further. For larger tensile strains, Pertsev *et al.*[33] predicted a phase where the polarization is directed along [110] (like ours), with an octahedral rotation around the same axis.

2. Dielectric properties

In this section, we compute the misfit strain dependence of the lattice contribution to the dielectric response ϵ in zero electric field; finite electric fields will be considered in the next section. First, we discuss separately the zone-center phonons and the Born effective charges that together determine ϵ according to Eq. (8).

The zone-center phonons of each phase are calculated at each misfit strain using density-functional perturbation theory. The lowest-frequency (softest) polar modes dominate the dielectric response, and we show the frequencies of the softest in-plane and out-of-plane transverse zone-center optical phonons as a function of misfit strain in Fig. 4. Their behavior reflects the phase transition sequence discussed in the previous section. By symmetry, these modes are degenerate at zero misfit strain. However, the lowest-frequency (or soft) mode polarized along [001] softens to zero as the misfit strain approaches the critical value of −0.75%, signaling the second-order transition from the paraelectric *P*4/*mmm* to the [001]-polarized *P*4*mm* structure. Similarly, the lowest-frequency in-plane soft mode softens to zero at +0.54% misfit strain, marking the second-order transition from *P*4/*mmm* to *Amm*2, which has its FE polarization along the [110] direction. As can be seen in the figure, the in-plane soft mode is only weakly affected at the *P*4/*mmm*-*P*4*mm* transition, while the out-of-plane soft mode shows a significant hardening in the *Amm*2 phase. The hardening is produced by coupling to the in-plane polarization that develops in the *Amm*2 phase. If the polarization is suppressed by keeping the atoms on their centrosymmetric positions, the mode evolves smoothly with increase of the in-plane lattice constant through the phase boundary, as is shown by the open circles in Fig. 4.

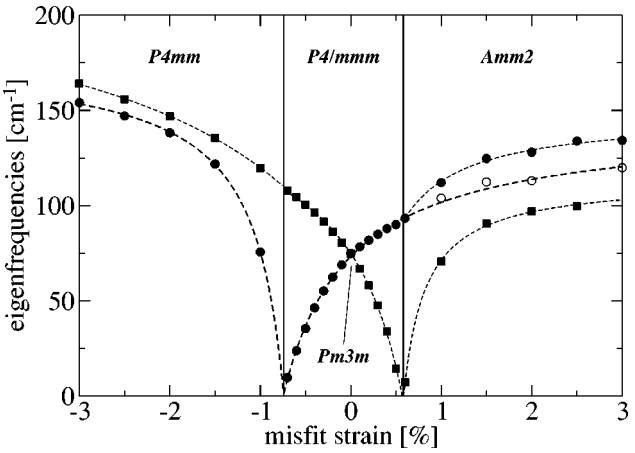

FIG. 4. FE soft-mode frequencies as a function of misfit strain. Solid circles indicate the FE soft mode polarized along [001]. Solid squares indicate the FE soft mode polarized along [110]. The vertical lines indicate the phase transition points at −0.75% and +0.54% misfit strain. Open circles denote the FE soft-mode frequency if the polarization along [110] is suppressed by keeping the atoms on their centrosymmetric positions.

We now examine the Born effective charge tensors Z_i^* as a function of misfit strain. In Fig. 5 we present, for brevity, only the Z_{11}^* and Z_{33}^* components of the tensors, where "1" and "3" refer to the [100] and [001] directions, respectively. While the Born effective charge tensors are not diagonal in the Cartesian frame in the *Amm*2 phase (whose principal axes, by symmetry, are along [110], $[1\bar{1}0]$, and [001]), the computed off-diagonal components (not shown) are found to be quite small. In what follows, O_1, O_2, and O_3 refer to the oxygen atoms forming Ti-O chains in the $\hat{x}$,$\hat{y}$, and $\hat{z}$ directions, respectively.

Figure 5 shows that in the paraelectric region, the Born effective charges are very close to the values for the cubic structure, 7.25 for Z_{33}^*(Ti) and −5.69 for $Z_{33}^*(O_3)$. As is well known, the fact that these are anomalous (in the sense of exceeding the nominal valence) arises from the hybridization of Ti and O orbitals in the Ti-O_3 chains and is quite sensitive to polar distortions of the chain.[45] Thus, in the ferroelectric phases, we expect a significant misfit strain dependence of the Born effective charges for these atoms. The effective charge of Ti, Z_{33}^*(Ti), drops by almost 16% in the ferroelectric region for compressive strain, with a corresponding increase of $Z_{33}^*(O_3)$. In comparison, Z^*(Sr) is rather insensitive to misfit strain over the whole region, showing a weak trend

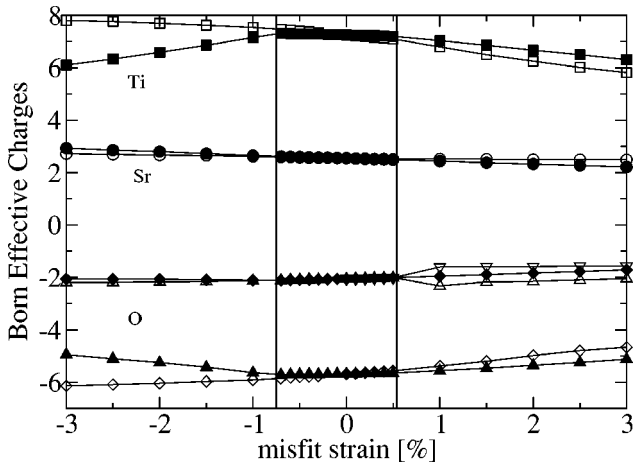

FIG. 5. Calculated Born effective charges Z^*_{33} (full symbols) and Z^*_{11} (open symbols) as a function of misfit strain. The cubic-structure values (at zero misfit strain) are $Z^*_{33}(\mathrm{Ti})=7.25$, $Z^*_{33}(\mathrm{Sr})=2.55$, $Z^*_{33}(\mathrm{O}_1)=-2.06$, and $Z^*_{33}(\mathrm{O}_3)=-5.69$. For O atoms, up-triangles represent O_3, down-triangles O_2, and diamonds O_1. [Full down-triangles are omitted in favor of full diamonds since $Z^*_{33}(\mathrm{O}_1)=Z^*_{33}(\mathrm{O}_2)$ everywhere; open down-triangles are omitted in favor of open up-triangles in the compressive region where $Z^*_{11}(\mathrm{O}_3)=Z^*_{11}(\mathrm{O}_2)$.]

towards lower values with increasing misfit strain.

In the tensile-strain-induced *Amm*2 ferroelectric phase, the orthorhombic symmetry (see Fig. 1) implies that $Z^*_{11}(\mathrm{O}_1)=Z^*_{22}(\mathrm{O}_2)\neq Z^*_{11}(\mathrm{O}_2)=Z^*_{22}(\mathrm{O}_1)$. In the range of strains shown, $Z^*_{11}(\mathrm{O}_1)$ shows a continuous increase of 18%, while the Z^*_{11} for O_2 and O_3 split slightly. The charge neutrality sum rule for the Z^* is maintained by a corresponding decrease for $Z^*_{11}(\mathrm{Ti})$.

In Fig. 6, we show the lattice contribution to the static dielectric response in zero electric field over the full range of computed misfit strains. The softening to zero frequency of the relevant phonons at the second-order phase boundaries

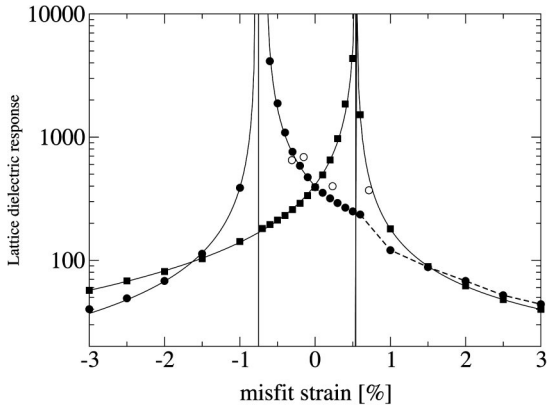

FIG. 6. Dielectric constant as a function of misfit strain. Solid circles and squares denote ϵ_{33} and ϵ_{11} respectively, where 3 always denotes the [001] direction and 1 refers to [100] in the *P*4*mm* region and [110] in the *Amm*2 region. Solid lines are fits proportional to $(\eta-\eta_c)^{-1}$, where η and η_c are the actual and critical misfit strains, respectively. Open circles are the ϵ_{33} measured by Hyun and Char (Ref. 14).

TABLE I. Normalized displacement vector ξ for selected strained states in the paraelectric phase.

Strain	u(Ti)	$u(\mathrm{O}_3)$	$u(\mathrm{O}_1)$
−0.7%	0.0929	−0.5081	−0.6055
−0.5%	0.0839	−0.5111	−0.6049
−0.3%	0.0726	−0.5129	−0.6049
−0.1%	0.0616	−0.5143	−0.6049
0.0%	0.0571	−0.5156	−0.6045
0.1%	0.0518	−0.5158	−0.6047
0.3%	0.0424	−0.5176	−0.6043
0.5%	0.0325	−0.5192	−0.6039

produces divergences in the dielectric response near the critical strains. These transitions show nearly perfect inverse-power-law behavior, except at the points closest to the phase transitions where the low eigenfrequencies lead to numerical inaccuracies. Throughout the paraelectric phase, both ϵ_{11} and ϵ_{33} are well over 100. The abrupt drop of ϵ_{33} in the tensile-strain region is related to the hardening of the lowest-frequency phonon polarized along [001] shown in Fig. 4. The comparison with the experimental data of Hyun and Char[14] will be discussed further in Sec. III B 2.

B. Response to electric field

Application of a finite electric field to epitaxially strained STO leads to changes in the structure and dielectric response that depend on misfit strain. In particular, the sensitivity to applied field is expected to be largest near the phase boundaries discussed above. In this section, we focus our attention on the strain regime corresponding to the zero-field paraelectric phase, with particular interest in the behavior as the transition to the *P*4*mm* phase is approached. This regime is most relevant to practical applications, as the ferroelectric state, its associated hysteresis, and the presence of ferroelectric domains are generally undesirable for tunable device applications. We also consider electric fields only along the [001] direction, in which case all displacements also occur only along [001].

To briefly recap our approach as presented in Sec. II C 2, we parametrize the electric field dependence of the atomic displacements up to fourth order. Combined with a linearized form of the functional dependence of the polarization on atomic displacement, this allows us to express the lattice contribution to the dielectric susceptibility in terms of the change in atomic displacements with electric field. We first discuss the displacements induced by the applied electric field, and then, in the following subsection, the resulting lattice contribution to the static dielectric response.

1. Structural properties

Using the approximate treatment of electric fields described in Sec. II C 1, we calculate the misfit-strain dependence of the displacement response to a small electric field. The resulting displacements, defined relative to the Sr atom,

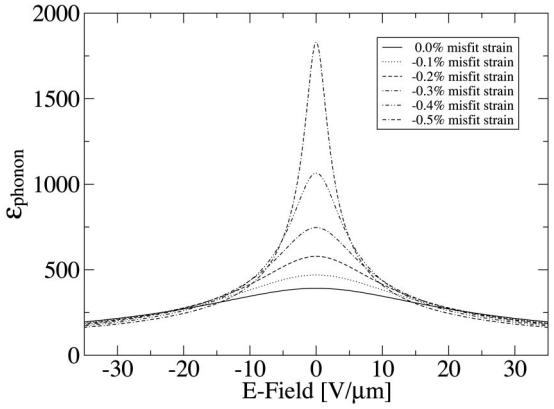

FIG. 7. Dielectric constant vs electric field for epitaxial STO in the paraelectric phase, for a series of compressive strains approaching the transition to the ferroelectric *P*4*mm* phase.

are then normalized to give the vector ξ reported in Table I for selected misfit strains. The O displacements in an electric field are relatively insensitive to misfit strain, while the Ti displacement in an electric field grows with in-plane compressive strain, reflecting the fact that in-plane compression, which is accompanied by a substantial expansion of the *c* lattice constant (see Fig. 3), leads to an opening of the oxygen octahedron in the *z*-direction and compression in the *xy* plane. The negative sign of the displacements of O atoms in a positive electric field results from the negative signs of their Born effective charges, while Ti is expected to exhibit a positive displacement since its Born effective charge is larger than that of Sr.

For the larger compressive strains in Table I, we find that our field-induced displacement vectors [Eq. (3)] are very similar to the atomic displacement patterns of the [001]-polarized soft mode at zero electric field. For example, the normalized atomic displacements of our computed normalized soft-mode eigenvector at −0.7% (near the critical misfit strain of −0.75%) are $(\mathrm{Ti},\mathrm{O}_3,\mathrm{O}_1)=(0.0910,-0.5103,-0.6081)$, almost identical to the displacement vector ξ at the same misfit strain. This shows that close to the phase boundary the structural response to an electric field is almost entirely dominated by the soft mode.

2. Dielectric properties and tunability

We now investigate the electric-field dependence of the lattice contribution to the dielectric response along the [001] direction as the in-plane compressive strain approaches the phase boundary with the *P*4*mm* phase. The results are shown in Fig. 7. As the magnitude of the misfit strain approaches the critical value of −0.75%, the dielectric response at low electric fields grows substantially.

We now gain further insight into our calculations through a quantitative comparison with experiment. The curves in Fig. 7 resemble Lorentzians, and this is expected from a phenomenological analysis, as follows.[46] Within the Landau-Devonshire formalism, the ferroelectric phase transition can be described by a free-energy functional *F* expanded about the paraelectric phase in even powers of the polarization *P*, i.e.,

$$F(P,T) = F_0 + AP^2 + BP^4 + CP^6 + \cdots . \tag{12}$$

The coefficients depend on misfit strain and temperature; *A* is generally assumed to have the strongest dependence, while the variation of *B* and higher order coefficients is small or even negligible. Keeping only terms in *F* to fourth order, the electric field is then given by

$$\mathcal{E} = \frac{\partial F}{\partial P} = 2AP + 4BP^3, \tag{13}$$

and the dielectric susceptibility by

$$\frac{1}{\chi} = \frac{\partial \mathcal{E}}{\partial P} = 2A + 12BP^2. \tag{14}$$

In the present discussion, the system is in the paraelectric phase $(A>0)$ so that these relations uniquely determine functions $P(\mathcal{E})$ and $\chi(\mathcal{E})$. From Eqs. (13) and (14), it is easy to see that in this fourth-order approximation we expect $\chi \rightarrow$ constant for $P\rightarrow 0$, while $\chi \propto \mathcal{E}^{-2/3}$ at large *P*. A useful approximate interpolation formula is then

$$\chi(\mathcal{E}) = \chi(0)\left[1+\left(\frac{\mathcal{E}}{\mathcal{E}_0}\right)^2\right]^{-1/3} \tag{15}$$

as has been used previously in the literature.[47,48] Making the approximation $\epsilon \gg 1$ so that $\epsilon \simeq 4\pi\chi$, we can write

$$\epsilon(\mathcal{E}) = \epsilon(0)\left[1+\left(\frac{\mathcal{E}}{\mathcal{E}_0}\right)^2\right]^{-1/3} \tag{16}$$

with $\epsilon(0)=4\pi\chi(0)$.

A detailed analysis shows that $\mathcal{E}_0 \propto \epsilon_0^{-3/2}$, where the constant of proportionality is determined by *B*, independent of *A*. That is, $\epsilon(0)^{3/2}\mathcal{E}_0$ is not expected to depend strongly on proximity to the ferroelectric phase transition, and thus is expected to vary only slowly with temperature and misfit strain, and to be only weakly affected by the LDA lattice-constant error. Fuchs *et al.*[48] used Eq. (16) to fit their experimentally-measured ϵ-vs-$\mathcal{E}$ data at 200 K, and they observe dielectric constants between 1480 and 5270; they find values of $\epsilon(0)^{3/2}\mathcal{E}_0$ ranging from 7.5 V/cm to 14.3 V/cm for films of 200–500 nm thickness. Fitting our theoretical data to the same form, we extract values of $\epsilon(0)^{3/2}\mathcal{E}_0$ ranging from 8.3 V/cm to 10.4 V/cm, in general agreement with the findings of Fuchs *et al.* The results of our comparison are summarized in Table II.

Hyun and Char[14] have grown $SrTiO_3$ on different substrates to investigate the influence of epitaxial strain on the tunability of $SrTiO_3$. For four samples, they report measurements at 77 K of in-plane lattice constants, c/a ratios, and dielectric constants, as summarized in Table III. There is good agreement between measured and calculated c/a ratios for the values of misfit strain observed in Ref. 14, as shown in Fig. 3. For three of the samples, the dielectric constant increases with compressive misfit strain in the paraelectric phase, in agreement with our calculations. The first sample is an exception: we expect it to exhibit a higher tunability,

TABLE II. Zero-field dielectric constant $\epsilon(0)$ and field scale $\mathcal{E}_0$ [reported as the slowly varying combination $\epsilon(0)^{3/2}\mathcal{E}_0$] obtained from the fit of Eq. (16) for each strain state in the paraelectric compressively-strained region.

Strain	$\epsilon(0)$	$\epsilon(0)^{3/2}\mathcal{E}_0$[V/cm]
0.0%	391	8.3
−0.1%	473	9.0
−0.2%	584	9.3
−0.3%	760	9.6
−0.4%	1088	10.0
−0.5%	1877	10.3
−0.6%	4125	10.1
−0.7%	19903	10.4

given its strain state. This discrepancy can be attributed to the poorer quality of samples grown on $LaAlO_3$.[14] Comparing our zero-temperature calculations in Table III with the measured value of 690 for the −0.1536% sample, and an additional computation of 319 for strain =+0.2% with the measured value of 400 for the +0.2305% sample (see Table III), we find surprisingly good agreement. This may be partly due to slight shifts in the experimental phase boundaries owing to finite temperature; because of our underestimate of lattice constants, our paraelectric phase is overstabilized, mimicking the effect of temperature and shifting the calculated phase boundary towards more compressive misfit strains.

Unlike the first three samples listed in Table III, which we expect to be paraelectric based on their in-plane lattice constants, the fourth sample should already be in the orthorhombic, tensile FE region, according to our calculations and to the phase diagram of Pertsev *et al.* For this reason, we did not include this experimental data point in Fig. 8. We should like to note, however, that the trends in the dependence of c/a and $\epsilon(0)$ on in-plane strain in Table III do not seem consistent regarding this last data point. As the strain changes from +0.23% to +0.72%, the measured c/a and $\epsilon(0)$ remain almost identical. The behavior of c/a, for example, seems inconsistent with the roughly linear dependence of c/a on misfit strain predicted in our Fig. 3, suggesting that more thorough checks of the experimental behavior in the region of strong tensile strain may be called for.

TABLE III. Measured misfit strain, c/a, and zero electric field dielectric constant for STO films on various substrates (Ref. 14) CRO and LAO stand for $CaRuO_3$ and $LaAlO_3$, respectively.

Strain	c/a	$\epsilon(\mathcal{E}=0)$	Materials
−0.3073%	1.0072	640	Au/STO/CRO/LAO
−0.1536%	1.0056	690	Au/STO/CRO/STO
+0.2305%	0.9937	400	Au/STO/SRO/LAO
+0.7170%	0.9942	360	Au/STO/SRO/STO

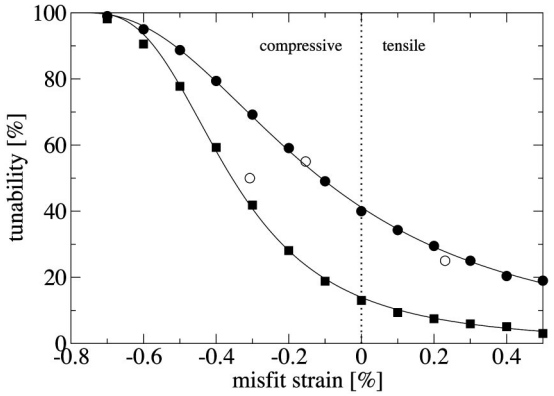

FIG. 8. Tunability $n=[\epsilon(0)-\epsilon(\mathcal{E})]/\epsilon(0)$ as a function of misfit strain. The values for $\epsilon(\mathcal{E})$ were taken at $\mathcal{E}=10$ V/μm (full squares), and $\mathcal{E}=25$ V/μm (full circles). Open circles are the experimental results of Hyun and Char for $\mathcal{E}=10$ V/μm.

Finally, we have calculated the strain dependence of the tunability parameter in the paraelectric phase for two different values of the bias field, $\mathcal{E}=10$ V/μm and $\mathcal{E}=25$ V/μm, with results shown in Fig. 8. Although a direct comparison is not possible because the theoretical and experimental conditions are rather different, the measurements of Hyun and Char for $\mathcal{E}=10$ V/μm are also shown. These results are closer to our calculated tunability for $\mathcal{E}=25$ V/μm than the one for $\mathcal{E}=10$ V/μm, consistent with the fact that our LDA-computed zero-temperature system is further from its ferroelectric transition (as indicated, e.g., by the smaller zero-field dielectric constant) than for the experimental system at 77 K, and therefore less tunable. Nevertheless, our results do tend to confirm that a substantial variation in the tunability can be attained by growing STO on substrates having different lattice constants.

IV. SUMMARY

In this work, we examined the effects of in-plane biaxial strain and an applied electric field on $SrTiO_3$ using first-principles density-functional theory within the local-density approximation. We computed the tunability of STO, and found this quantity to be highly sensitive to epitaxial strain. We also find that the dielectric constant itself varies significantly with strain, and for sufficiently large compressive strains, STO can be made ferroelectric with a polarization similar to that of bulk $BaTiO_3$. Our results are in good agreement with available experiments.

Our studies complement and extend previous theoretical work on STO films using a phenomenological Landau theory. Our parameter-free description provides structural parameters and phonon frequencies that can be compared with future experiments; in addition, we observe significant differences between our zero-temperature phase diagram and that obtained using Landau theories fit to empirical data.

These results should be useful for the analysis of ultrathin epitaxial films and superlattice structures involving STO. In the latter, high strain states, achieved through layering, can result in novel artificial materials with enhanced properties

over those of their bulk constituents, as was recently predicted for $BaTiO_3/SrTiO_3$ superlattices.[49]

For coherent epitaxial systems more complex than STO and at finite temperatures, it seems clear that epitaxial strain will generally be a crucial factor in determining properties. In particular, we expect our results for STO to be a useful guide in understanding the strain dependence of more complex ferroelectric thin films with high tunability, such as BST.

ACKNOWLEDGMENTS

This work was supported by ONR N00014-01-1-1061 and ONR N00014-00-1-0261.

*Electronic address: a.antons@fz-juelich.de; Present address: Institut of Solid State Research (IFF), Research Centre Jülich, 52425 Jülich, Germany.

†Present address: The Molecular Foundry, Materials Sciences Division, Lawrence Berkeley National Laboratory, Berkeley, California 94720, USA.

[1] S. J. Fiedziuszko, I. C. Hunter, T. Itho, Y. Kobayashi, T. Nishikawa, S. N. Stitzer, and K. Wakino, IEEE Trans. Microwave Theory Tech. **50**, 706 (2002).

[2] V. K. Varadan, D. K. Gohdgaonkar, V. V. Varadan, J. F. Kelly, and P. Glikerdas, Microwave J. **35** (1), 116 (1992).

[3] J. S. Horwitz, D. B. Chrisey, J. M. Pond, R. C. Y. Auyeung, C. M. Cotell, K. S. Grabowski, P. C. Dorsey, and M. S. Kluskens, Integr. Ferroelectr. **8**, 53 (1995).

[4] Y. Yoneda, K. Sakaue, and H. Terauchi, Surf. Sci. **529**, 283 (2003).

[5] W. Qing, W. Lian-wei, X. Shuo, S. Qin-wo, and L. Cheng-lu, J. Funct. Mater. **8**, 128 (2002).

[6] Y. Gim, T. Hudson, Y. Fan, C. Kwon, A. T. Findikoglu, B. J. Gibbons, B. H. Park, and Q. X. Jia, Appl. Phys. Lett. **77**, 1200 (2000).

[7] L. A. Knauss, J. M. Pond, J. S. Horowitz, D. B. Chrisey, C. H. Mueller, and R. Treece, Appl. Phys. Lett. **69**, 25 (1996).

[8] C. L. Canedy, H. Li, S. P. Alpay, L. Salamanca-Riba, A. L. Roytburd, and R. Ramesh, Appl. Phys. Lett. **77**, 1695 (2000).

[9] N. A. Pertsev, A. G. Zembilgotov, and A. K. Tagantsev, Phys. Rev. Lett. **80**, 1988 (1998).

[10] A. R. James and X. X. Xi, J. Appl. Phys. **92**, 6149 (2002).

[11] B. H. Park, E. J. Peterson, Q. X. Jia, J. Lee, X. Zeng, W. Si, and X. X. Xi, Appl. Phys. Lett. **78**, 533 (2001).

[12] Z.-G. Ban and S. P. Alpay, J. Appl. Phys. **93**, 504 (2003).

[13] H. C. Li, W. Si, A. D. West, and X. X. Xi, Appl. Phys. Lett. **73**, 190 (1998).

[14] S. Hyun and K. Char, Appl. Phys. Lett. **79**, 254 (2001).

[15] J. H. Haeni, P. Irvin, W. Chang, R. Uecker, P. Reiche, Y. L. Li, S. Choudhury, W. Tian, M. E. Hawley, B. Craigo, A. K. Tagantsev, X. Q. Pan, S. K. Streiffer, L. Q. Chen, S. W. Kirchoefer, J. Levy, and D. G. Schlom, Nature (London) **430**, 758 (2004).

[16] P. A. Fleury, J. F. Scott, and J. M. Worlock, Phys. Rev. Lett. **21**, 16 (1968).

[17] A. S. Chaves, F. C. S. Barreto, and L. A. A. Ribeiro, Phys. Rev. Lett. **37**, 618 (1976).

[18] R. Migoni, H. Bilz, and D. Bäuerle, Phys. Rev. Lett. **37**, 1155 (1976).

[19] K. A. Müller and H. Burkard, Phys. Rev. B **19**, 3593 (1979).

[20] K. A. Müller, W. Berlinger, and E. Tosatti, Z. Phys. B: Condens. Matter **84**, 277 (1991).

[21] R. Martonák and E. Tosatti, Phys. Rev. B **49**, 12 596 (1994).

[22] W. Zhong and D. Vanderbilt, Phys. Rev. B **53**, 5047 (1996).

[23] W. Zhong and D. Vanderbilt, Phys. Rev. Lett. **74**, 2587 (1995).

[24] R. A. Cowley, Phys. Rev. **134**, A981 (1964).

[25] J. M. Worlock, in *Structural Phase Transitions and Soft Modes*, edited by E. J. Samuelsen, E. Andersen, and J. Feder (Universitetsforlaget, Oslo, 1971).

[26] H. Uwe and T. Sakudo, Phys. Rev. B **13**, 271 (1976).

[27] R. D. King-Smith and D. Vanderbilt, Phys. Rev. B **49**, 5828 (1994).

[28] C. LaSota, C. Z. Wang, R. Yu, and H. Krakauer, Ferroelectrics **194**, 109 (1997).

[29] C. LaSota, C. Z. Wang, R. Yu, and H. Krakauer, in *First-Principles Calculations for Ferroelectrics: Fifth Williamsburg Workshop*, edited by R. E. Cohen (AIP, Woodbury, NY, 1998), p. 139.

[30] W. Zhong, D. Vanderbilt, and K. M. Rabe, Phys. Rev. Lett. **73**, 1861 (1994).

[31] N. Sai and D. Vanderbilt, Phys. Rev. B **62**, 13 942 (2000).

[32] N. A. Pertsev, A. K. Tagantsev, and N. Setter, Phys. Rev. B **61**, R825 (2000).

[33] N. A. Pertsev, A. K. Tagantsev, and N. Setter, Phys. Rev. B **65**, 219901 (E) (2002).

[34] S. Baroni, A. Dal Corso, S. de Gironcoli, and P. Giannozzi, http://www.pwscf.org

[35] D. Vanderbilt, Phys. Rev. B **41**, 7892 (1990).

[36] H. J. Monkhorst and J. D. Pack, Phys. Rev. B **13**, 5188 (1976).

[37] N. Sai, K. M. Rabe, and D. Vanderbilt, Phys. Rev. B **66**, 104108 (2002).

[38] I. Souza, J. Íñiguez, and D. Vanderbilt, Phys. Rev. Lett. **89**, 117602 (2002).

[39] P. Umari and A. Pasquarello, Phys. Rev. Lett. **89**, 157602 (2002).

[40] K. M. Rabe, MRS Proc. 718, edited by K. Poeppelmeier, A. Navrotsky, and R. Wentzcovitch (Materials Research Society, 2002).

[41] H. Fu and L. Bellaiche, Phys. Rev. Lett. **91**, 257601 (2003).

[42] To be precise, the electrostatic part of $E_{KS}(\mathcal{E})$ is defined here as the unit-cell integral of $[\Delta\mathcal{E}_{mic}(\mathbf{r})]^2/8\pi$, where $\Delta\mathcal{E}_{mic}(\mathbf{r}) = \mathcal{E}_{mic}(\mathbf{r}) - \mathcal{E}$ is the difference between the microscopic and macroscopic fields.

[43] The accuracy of the lattice susceptibility when computed in this manner depends on the fit of the energy expansion coefficients in Eq. (6). At compressive strains near the ferroelectric phase transition, the energy as expressed in Eq. (4) has a very small quadratic coefficient b, and is thus increasingly difficult to fit reliably. This is especially problematic because, as can be seen from Eqs. (6) and (11), the dielectric constant in zero electric field depends only on the quadratic term in the energy expansion. Thus, for compressive strains larger than 0.4%, we adjust b

so that the zero-field dielectric constant obtained from (11) agrees with that obtained from DFPT. For these strain values, only the fourth order coefficient *d* is fitted using the energy expansion.

[44] R. D. King-Smith and D. Vanderbilt, Phys. Rev. B **47**, 1651 (1993).

[45] W. Zhong, D. Vanderbilt, R. D. King-Smith, and K. M. Rabe, Ferroelectrics **164**, 291 (1995).

[46] A. F. Devonshire, Philos. Mag. **40**, 1040 (1949).

[47] R. Auer, E. Brecht, K. Herrmann, and R. Schneider, Physica C **299**, 177 (1998).

[48] D. Fuchs, C. W. Schneider, R. Schneider, and H. Rietschel, J. Appl. Phys. **85**, 7362 (1999).

[49] J. B. Neaton and K. M. Rabe, Appl. Phys. Lett. **82**, 1586 (2003).